Reaction Mechanisms

DOI: 10.1002/anie.201308431

Spectroscopic and Computational Study of a Nonheme Iron Nitrosyl Center in a Biosynthetic Model of Nitric Oxide Reductase**

*Saumen Chakraborty, Julian Reed, Matthew Ross, Mark J. Nilges, Igor D. Petrik, Soumya Ghosh, Sharon Hammes-Schiffer, J. Timothy Sage, Yong Zhang, Charles E. Schulz, and Yi Lu**

Abstract: *A major barrier to understanding the mechanism of nitric oxide reductases (NORs) is the lack of a selective probe of NO binding to the nonheme Fe_B center. By replacing the heme in a biosynthetic model of NORs, which structurally and functionally mimics NORs, with isostructural ZnPP, the electronic structure and functional properties of the Fe_B nitrosyl complex was probed. This approach allowed observation of the first S = 3/2 nonheme {FeNO}^{7} complex in a protein-based model system of NOR. Detailed spectroscopic and computational studies show that the electronic state of the {FeNO}^{7} complex is best described as a high spin ferrous iron (S = 2) antiferromagnetically coupled to an NO radical (S = 1/2) [Fe^{2+}-NO•]. The radical nature of the Fe_B-bound NO would facilitate N–N bond formation by radical coupling with the heme-bound NO. This finding, therefore, supports the proposed trans mechanism of NO reduction by NORs.*

Nitric oxide reductases (NORs) catalyze two-electron reductions of nitric oxide to nitrous oxide ($2NO + 2H^+ + 2e^- \rightarrow N_2O + H_2O$), a critical step in the biological denitrification process.[1] Additionally, many pathogenic non-denitrifying bacteria use NORs to inactivate NO produced by the host's immune system.[2] Thus, understanding the nitrosyl complexes of the enzyme and their role in the NO reduction mechanism is not only of biochemical significance, but also has broad implications for the global nitrogen cycle. Bacterial NORs are integral membrane proteins which contain a binuclear active site consisting of a high-spin (HS) heme b_3 and a nonheme iron (Fe_B) center. Three mechanisms of NO reduction to form N_2O have been proposed: the *cis*-heme b_3, *cis* Fe_B, and *trans* mechanisms (see Scheme S1 in the Supporting Information).[1a,3] Important to differentiating these mechanisms is the study of nitrosyl complexes of both the heme and the Fe_B center. Spectroscopic features for the heme nitrosyl complexes in NORs have been probed. However, those of the Fe_B nitrosyl complexes have been elusive because its spectroscopic signatures are often masked by those of the high affinity heme nitrosyl (K_{eq} for NO binding to ferrous hemes is ca. 10^{10}–$10^{12}\,M^{-1}$).[4] Therefore, this issue has become one of the most critical barriers to our current understanding of the electronic structure and reaction mechanism of NORs. Because NORs are integral membrane proteins, their heme cofactor(s) cannot be successfully replaced to probe the effect of NO binding to the Fe_B site selectively.

Several studies have elucidated the electronic and spectroscopic properties of heme nitrosyl complexes.[5] In addition, synthetic models of NORs have been reported.[6] To complement the studies of native NORs and synthetic models, we have taken advantage of small, easy-to-prepare, and well-characterized proteins such as myoglobin to obtain biosynthetic models of NORs.[7] Using such an approach, we have successfully engineered an Fe_B site in the distal pocket of sperm whale myoglobin (swMb). These designed proteins, Fe_BMb1 (L29H, F43H, H64, V68E swMb),[7a] and Fe_BMb2 (I107E Fe_BMb1)[7c] not only reproduced the active-site structure of NORs, such as the cytochrome-*c*-dependent NOR (cNOR),[8] but also displayed NOR activity.

One of the major advantages of using biosynthetic model proteins is that the heme can be readily replaced with isostructural Zn/protoporphyrin IX (ZnPP), thus allowing us to spectroscopically probe the effect of NO binding to the Fe_B site exclusively. Herein, we report the preparation of Fe^{II}-ZnPPFe_BMb1, where the Fe^{II} is in the Fe_B center and the heme in Fe_BMb1 is substituted with ZnPP, as confirmed by X-ray crystallography. Spectroscopic studies of Fe^{II}-ZnPPFe_BMb1 and its NO complex by UV/Vis absorption, electron paramagnetic resonance (EPR), and Mössbauer spectroscopic methods, in conjunction with DFT analysis, have allowed us to gain insight into the NOR reaction mechanism. This study is the first report where the Fe_B

[*] Dr. S. Chakraborty, J. Reed, M. Ross, Dr. M. J. Nilges, I. D. Petrik, Dr. S. Ghosh, Prof. Dr. S. Hammes-Schiffer, Prof. Dr. Y. Lu
Department of Chemistry and Biochemistry, University of Illinois at Urbana-Champaign, Urbana, IL (USA)
E-mail: yi-lu@illinois.edu
Prof. Dr. J. T. Sage
Department of Physics, Northeastern University
Boston, MA (USA)
Prof. Dr. Y. Zhang
Department of Chemistry, Chemical Biology and Biomedical Engineering, Stevens Institute of Technology, Hoboken, NJ (USA)
Prof. Dr. C. E. Schulz
Department of Physics, Knox College
Galesburg, IL (USA)

[**] This work is supported by the US National Institute of Health (5T32-GM070421 to J.R., GM056207 to S.H.S., GM085774 to Y.Z., and GM062211 to Y.L.) and the National Science Foundation (CHE-1026369 to J.T.S.). We thank Dr. Sebastian Stoian for helpful discussions and Prof. Eric Oldfield for access to their glove bag in a cold room.

Supporting information for this article (details of protein expression and purification, reconstitution of Fe_BMb1 with ZnPP, experimental details of determination of molar absorptivity, synthesis of $^{57}FeCl_2$, Fe^{II} titration, EPR, Mössbauer sample preparation and data analysis, X-ray crystallography, ICP, and QM/MM calculations) is available on the WWW under http://dx.doi.org/10.1002/anie.201308431.

nitrosyl complex of NOR or its models have been probed exclusively in a protein system, and the results support the *trans* mechanism of the NOR reaction.

Fe_BMb1 was prepared as reported previously.[7a] After extracting its heme using a slightly modified method from that in the literature (see the Supporting Information),[10] the protein was reconstituted with ZnPP (Figure 1). The UV/Vis spectrum of ZnPP-reconstituted protein, ZnPPFe_BMb1, has absorption peaks at $\lambda = 427$, 553, and 595 nm (Figure 2). These spectral features are different from those of ZnPP

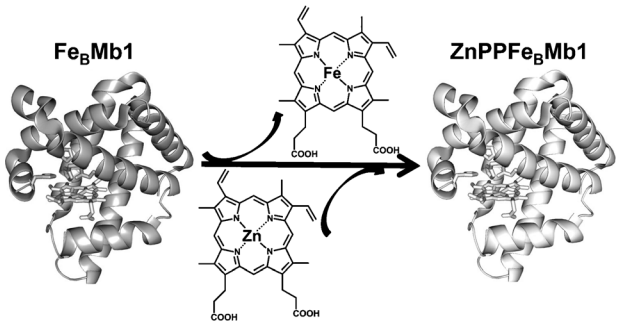

Figure 1. Replacement of heme in Fe_BMb1 with ZnPP, thus yielding ZnPPFe_BMb1. Figures were generated in PyMol[9] using PDB codes 3K9Z[7a] and 4MXL, respectively.

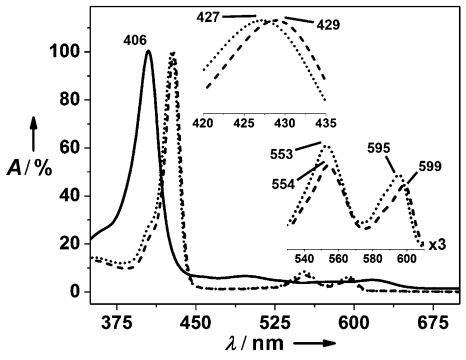

Figure 2. UV/Vis spectra of Fe_BMb1 (solid line), ZnPPFe_BMb1 (dotted line), and ZnPPFe_BMb1 in the presence of 1.0 equiv Fe^{II} (dashed line) in 50 mM Bis-Tris buffer pH 7.3. Peak positions in the Soret and visible region of ZnPPFe_BMb1 and Fe^{II}-ZnPPFe_BMb1 are shown as insets.

alone (see Figure S1), or from Fe_BMb1 which contains heme (Figure 2), thus suggesting that the non-native cofactor ZnPP was successfully incorporated into Fe_BMb1. To obtain further evidence of successful incorporation of the ZnPP into Fe_BMb1, an X-ray structure of ZnPPFe_BMb1, refined to 1.5 Å resolution, was obtained (see Figure S2) and shows successful incorporation of the non-native cofactor.

Having established that Fe_BMb1 can be reconstituted with ZnPP, Fe^{II} binding to the Fe_B site of ZnPPFe_BMb1 was probed by UV/Vis spectroscopy. As shown in Figure 2, addition of 1.0 equivalent of $FeCl_2$ to 7 μM ZnPPFe_BMb1 in 50 mM Bis-Tris pH 7.3 resulted in a red shift of the Soret band from $\lambda =$ 427 nm to $\lambda = 429$ nm and concomitant changes in the visible region of the spectra, with isosbestic points occurring at $\lambda =$ 432, 562, and 598 nm (see Figure S3). As the electronic environment around the ZnPP framework is being perturbed upon Fe^{II} binding at the distal pocket, only slight changes in the wavelength maxima are expected to be observed.[7a,c,d,11] By following the spectral changes upon Fe^{II} addition (Figure S3), a dissociation constant (K_d) of (7.2 ± 0.4) μM for Fe^{II} binding to the Fe_B site of ZnPPFe_BMb1 was obtained. Interestingly, compared to the K_d of (21.5 ± 0.5) μM for the same Fe_BMb1 but with heme in the active site (see Figure S4), these data suggest that substitution of heme with ZnPP into Fe_BMb1 increases Fe^{II} binding affinity at the Fe_B site by about threefold.

The Fe^{II} binding was further investigated by crystallography. A 1.52 Å resolution X-ray structure of the $FeCl_2$-soaked crystal of ZnPPFe_BMb1 clearly shows that a metal is present at the Fe_B site. Anomalous X-ray scattering data of the crystals collected above Fe K-edge at 7.2 keV unambiguously assigned this metal to be Fe (Figure 3). Furthermore, anomalous data collected below the Fe K-edge at 7.0 keV did

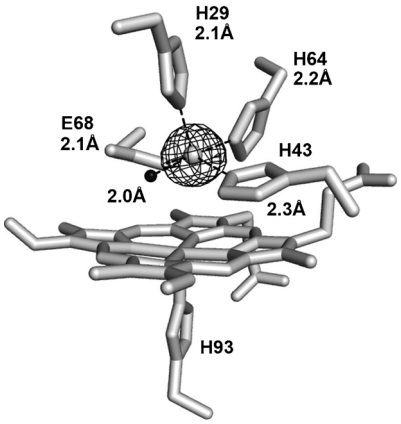

Figure 3. 1.52 Å X-ray structure of Fe^{II}-ZnPPFe_BMb1. ZnPP and the coordinating residues are shown as sticks. Fe is shown as gray sphere and the water molecule is shown as black sphere. The anomalous map generated in PHENIX[12] from the data collected at the Fe K-edge at 7.2 keV is drawn at 7σ and shown as gray mesh. $R_{fac} = 0.18$, $R_f = 0.22$. Figure was generated using PyMol.[9] PDB ID 4MXK.

not show the presence of any anomalous electron density at the Fe_B site (see Figure S5 in the Supporting Information), thus ruling out the possibility of any other metal ion at the Fe_B site. Structural overlays of Fe^{II}-ZnPPFe_BMb1 with the active sites of Fe^{II}-Fe_BMb1[7a] and cNOR[8] demonstrated that these structures were strikingly similar to each other (Figure 4). Therefore, the Fe_B site of Fe^{II}-ZnPPFe_BMb1 is a structural analogue of the nonheme site of cNOR and Fe_BMb1. The close structural similarity between Fe^{II}-ZnPPFe_BMb1 and Fe^{II}-Fe_BMb1 also suggests that the threefold higher affinity of Fe^{II} in the former was likely influenced by changes in the electronic environment around the metal-binding site caused by replacement of iron protoporphyrin IX with ZnPP, and not by the changes in the overall structure of the Fe_B site.

We next studied NO binding properties of Fe^{II}-ZnPPFe_BMb1 by EPR spectroscopy. The sample containing Fe^{II}-ZnPPFe_BMb1 in the absence of NO had no detectable

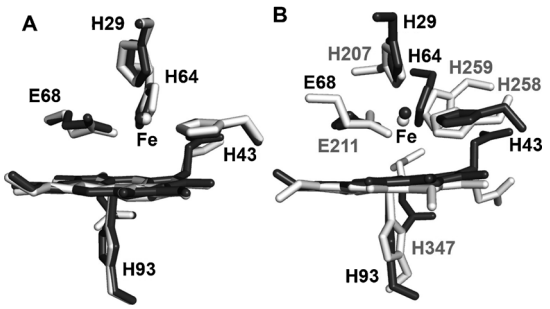

Figure 4. Overlay of Fe^{II}-ZnPPFeBMb1 (PDB ID: 4MXK, dark gray) with Fe^{II}-FeBMb1 (PDB ID: 3K9Z, light gray) (A), and cNOR (PDB ID: 3O0R, light gray) (B). Figures were generated using PyMol.

EPR signal (see Figure S6). With addition of up to 5 equivalents of NO, the major peak observed was a radical-like signal at $g \approx 2.01$, with no other significant spectral features (see Figure S7). However, in the presence of 10 equivalents of NO, an EPR feature at $g \sim 4.04$ appeared, thus indicating the formation of a new species. Similar features were also present in the presence of 20 equivalents of NO. Encouraged by the results, we collected EPR spectrum under the conditions to maximize the signal of this new species ($T = 5$ K, power = 20 dB). The resulting spectrum shows two well-resolved doublets 1_x,1_y, and 2_x,2_y at $g = 4.36$, 3.58, and 4.13, 3.73, respectively (Figure 5, Table 1). No other features were observed at lower field (see Figure S8). The EPR spectrum

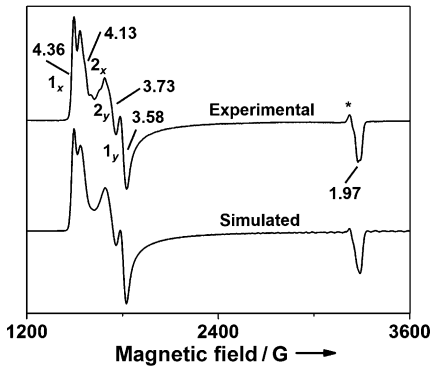

Figure 5. X-band EPR spectrum of a sample containing 0.7 mM $ZnPPFe_BMb1$ in the presence of 1.0 equiv $FeCl_2$ and 20 equiv of NO in 50 mM Bis-Tris buffer pH 7.3, and the simulated spectrum. Excess NO was used to ensure saturation of the Fe_B site. Experimental parameters: $T = 5$ K, microwave frequency = 9.053 GHz, microwave power = 20 dB, modulation amplitude = 4 G. g values and the components are labeled. *A radical-type peak (< 1%).

Table 1: Parameters extracted from fitting of the EPR spectrum in Figure 5.

Peaks	g_x	g_y	g_z	[%]	E/D
1_x,1_y	1.985	1.985	1.987	46[a]	0.063
2_x,2_y	1.987	1.987	1.987	54[b]	0.040

[a,b] The ferrous nitrosyl complex is present in two rhombic geometries with $E/D = 0.063$, and 0.040, respectively. $D = 7.2$ cm^{-1} as obtained from the Mössbauer measurements (see Table S3) were used to simulate the EPR spectrum.

was simulated as a $\{FeNO\}^7$ ferrous nitrosyl complex with an $S = 3/2$ ground state according to Enemark–Feltham nomenclature.[13] The sharp outer doublet 1_x,1_y, accounting for 46% of the spin, is more rhombic with an E/D = 0.063 than the major (54%) broad inner doublet 2_x,2_y which has an E/D of 0.040. The corresponding $g_{\|}$ components are not well resolved in the region of $g \sim 1.97$. The two different components can be ascribed to either different orientations of NO bound to the Fe_B site, or slight changes in the orientation of Fe^{II} ligands upon NO binding. Multiple Fe-NO symmetries with different rhombicities are commonly observed in heme nitrosyls.[5g,14] To test whether different components of the Fe_B-NO complex observed here are a result of hyperfine interaction with the ^{14}N nucleus, EPR simulations were performed taking into consideration this interaction. The data in Figure S9 rules out this possibility as a satisfactory fit was not obtained. Detailed characterization of the saturation behavior of the radical-like signal at $g \sim 2.01$ shows that it is not a "free" radical, instead it is most likely a radical associated with a metal ion (see Figures S10–12, and Tables S1 and S2).

Freeze-quench EPR studies of the reaction of reduced NOR from *P. aeruginosa*[15] with NO-saturated buffer showed a peak at $g = 4$ within 0.5 milliseconds of mixing, corresponding to about a 30% population of the Fe_B nitrosyl $\{FeNO\}^7$ complex with a $S = 3/2$ ground state. Similar EPR features have been reported for the reaction of NO with various nonheme iron proteins,[16] as well as model complexes.[6b,17] ICP-MS analysis and spin quantification against Fe^{III}-EDTA gave 61% of the total $S = 3/2$ species in Fe^{II}-$ZnPPFe_BMb1$-NO. These results, therefore, suggest that the $S = 3/2$ Fe_B-NO complex can be formed in heme-substituted Fe^{II}-$ZnPPFe_BMb1$. Control experiments containing $ZnPPFe_BMb1$ and NO in the absence of Fe^{II} in the Fe_B site did not show any EPR feature (see Figure S13), thus confirming that the aforementioned EPR feature of the $S = 3/2$ ferrous nitrosyl species can be observed only when NO is present with the Fe_B site reconstituted by Fe^{II}.

To understand the electronic and spin state of the Fe_B nitrosyl species further, we carried out field-dependent Mössbauer measurements at 4.2 K. In the absence of NO, a sample containing 3.5 mM $^{57}Fe^{II}$-$ZnPPFe_BMb1$ shows a single quadrupole doublet at 0.01 Tesla (T) (see Figure S14). In the presence of a magnetic field (1–9 T) the doublet splits into multiplets, resulting from magnetic hyperfine interactions with the electron spin. A quadrupole splitting $(\Delta E_Q) = (2.85 \pm 0.01)$ mm s^{-1}, and isomer shift $\delta_{Fe} = (1.13 \pm 0.01)$ mm s^{-1} are obtained from fits indicative of a high-spin ferrous ($S = 2$) species (Table 2 and Table S3).[18] Similar parameters have been reported for nonheme ferrous sites in proteins.[16a] In the presence of 20 equivalents NO, the Mössbauer spectrum (Figure 6) of $^{57}Fe^{II}$-$ZnPPFe_BMb1$-NO at low field (0.01 T) shows two doublets (solid and dashed gray lines), and a magnetically split component (gray dots). The solid gray line in the 0.01 T field spectrum represents 35% of unreacted Fe^{II} species. To simplify the high-field spectra, this unreacted component was subtracted, and the splitting pattern of the 65% iron nitrosyl component is shown in Figure 6. Simultaneous least-squares fits to the three applied field spectra gave Mössbauer parameters $(\Delta E_Q) =$

Table 2: Experimental and calculated (parentheses) Mössbauer parameters of ^{57}Fe-ZnPPFe$_B$Mb1 in the absence and presence of NO. Experimental conditions: $T = 4.2$ K, field = 0.01 T, 1 T, 5 T, 9 T.

Sample	δ_{Fe} [mm s^{-1}]	ΔE_Q [mm s^{-1}]	S	Fe spin population	NO spin population
^{57}Fe-ZnPPFe$_B$Mb1	1.13 (1.13)[a]	2.85 (3.15)[a]	2	3.75[b]	n.a.
^{57}Fe-ZnPPFe$_B$Mb1-NO	0.69 (0.70)[a]	−1.70 (−2.01)[a]	3/2	3.66[b]	−0.90[b]

[a] Mössbauer parameters were calculated from active site model. [b] Spin populations were calculated from QM/MM calculations. n.a. = not applicable.

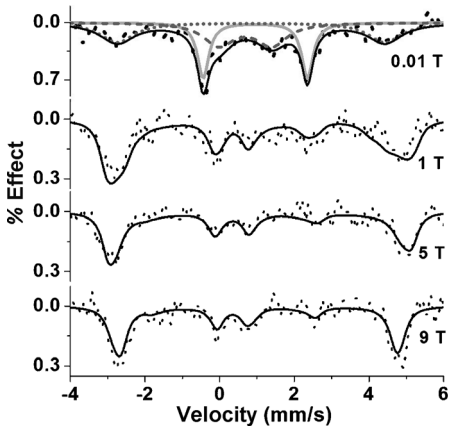

Figure 6. Field-dependent Mössbauer spectra of a sample containing 7 mM ^{57}Fe^{II}-ZnPPFe$_B$Mb1, and 20 equiv of NO in 50 mM Bis-Tris pH 7.3, collected at 4.2 K. Black dots: experimental data, black lines: sum of fit, gray solid line: ferrous $S = 2$ starting material, gray dashes: $S = 3/2$ {FeNO}^{7} component in intermediate relaxation, gray short dots: magnetically split $S = 3/2$ {FeNO}^{7} component. Only the splitting pattern of 65% of the $S = 3/2$ {FeNO}^{7} species is shown in high field. The $S = 3/2$ species at all fields was simulated using a slow relaxation model. The $S = 2$ species at low field was simulated as Lorentzian. (See Figure S15 for a color representation of this figure).

(-1.70 ± 0.01) mm s^{-1}, and $\delta_{Fe} = (0.69 \pm 0.01)$ mm s^{-1}, which are indicative of an $S = 3/2$ six-coordinate {FeNO}^{7} species (Tables 2 and S3), and found in other proteins as well as small-molecule models.[16a,d,17d,19]

Some of the $S = 3/2$ species (gray dashed line) is in intermediate relaxation at low field (0.01 T), and is most likely due to the proximity to the small population of the metal-associated radical species detected by EPR (see the Supporting Information). In the applied field, this $S = 3/2$ component is at the slow relaxation limit and is therefore indistinguishable to the other $S = 3/2$ center (gray dots, 0.01 T) which is already in the slow relaxation regime. Simulations to the high-field spectra show excellent matches to the positions and intensity of all the spectral features, thus supporting that there is only a single type of $S = 3/2$ species. These conclusions are supported by low-field Mössbauer data obtained under lower NO equivalents at higher temperatures (see Figure S16 and Table S4).

The electronic state of the $S = 3/2$ {FeNO}^{7} species in both proteins and model complexes has been most frequently described as a result of antiferromagnetic coupling of HS ferric ($S = 5/2$) to NO$^-$ ($S = 1$) [Fe^{3+}-NO$^-$][16f,17b,d] or as antiferromagnetic coupling of HS ferrous ($S = 2$) to NO radical ($S = 1/2$) [Fe^{2+}-NO$^\bullet$].[16a,19c,20] To obtain further insight into the electronic structure of the {FeNO}^{7} moiety, we calculated the Mulliken spin populations (Table 2) at the Fe and NO centers of the structures obtained from quantum mechanical/molecular mechanical (QM/MM) calculations as well as partially optimized active-site structures (see Figures S17 and S18). In these structures, NO occupies the vacant axial coordination site as the sixth ligand to Fe$_B$. The Mulliken spin population on the Fe$_B$ center remains virtually the same in the absence and presence of NO, at 3.75 and 3.66, respectively, thus indicating four unpaired electrons, while the spin population on NO is found to be −0.90, thus indicating one unpaired electron. These results unambiguously support the assignment of a HS ferrous center ($S = 2$) antiferromagnetically coupled to an NO radical ($S = 1/2$) [Fe^{2+}-NO$^\bullet$]. Furthermore, we computed the Mössbauer parameters at the Fe$_B$ site in the absence and presence of NO for partially optimized active-site structures (see the Supporting Information for details). As can be seen from Table 2, both the calculated ΔE_Q and δ_{Fe} values agree well with the experimental data.

In conclusion, we have succeeded in probing the NO binding properties of the Fe$_B$ site in a biosynthetic model protein of NOR by replacing the high affinity heme with isostructural ZnPP in the protein ZnPPFe$_B$Mb1. Such feats are not easily achievable in native NORs, as these are complex membrane proteins with multiple heme cofactors. Structural overlays with cNOR clearly show that the Fe$_B$ site in Fe^{II}-ZnPPFe$_B$Mb1 is a structural mimic of the Fe$_B$ site in the native enzyme. EPR spectral studies show that NO binding to the Fe$_B$ site yields rhombic signals corresponding to a {FeNO}^{7} $S = 3/2$ ferrous nitrosyl complex. Mössbauer and QM/MM studies were used to confirm the electronic properties of the {FeNO}^{7} complex in Fe^{II}-ZnPPFe$_B$Mb1-NO as HS ferrous ($S = 2$) antiferromagnetically coupled with NO radical ($S = 1/2$) [Fe^{2+}-NO$^\bullet$]. This exciting finding indicates that the radical nature of the NO would facilitate the radical coupling of the second heme-bound NO to promote N–N bond formation, thus supporting the proposed *trans* mechanism of NO reduction by NORs.[1b,6,15,21]

Received: September 26, 2013
Revised: November 27, 2013
Published online: January 31, 2014

Keywords: computational chemistry · EPR spectroscopy · heme proteins · iron · reaction mechanisms

[1] a) Y. Shiro, H. Sugimoto, T. Tosha, S. Nagano, T. Hino, *Philos. Trans. R. Soc. London Ser. B* **2012**, *367*, 1195–1203; b) M. P. Schopfer, J. Wang, K. D. Karlin, *Inorg. Chem.* **2010**, *49*, 6267–6282; c) I. M. Wasser, S. de Vries, P. Moënne-Loccoz, I. Schröder, K. D. Karlin, *Chem. Rev.* **2002**, *102*, 1201–1234.

[2] a) J. R. Laver, T. M. Stevanin, S. L. Messenger, A. D. Lunn, M. E. Lee, J. W. Moir, R. K. Poole, R. C. Read, *FASEB J.* **2010**,

24, 286 – 295; b) T. M. Stevanin, J. W. Moir, R. C. Read, *Infect. Immun.* **2005**, *73*, 3322 – 3329.
[3] a) P. Möenne-Loccoz, *Nat. Prod. Rep.* **2007**, *24*, 610 – 620; b) N. Xu, A. L. O. Campbell, D. R. Powell, J. Khandogin, G. B. Richter-Addo, *J. Am. Chem. Soc.* **2009**, *131*, 2460 – 2461.
[4] L. E. Goodrich, F. Paulat, V. K. K. Praneeth, N. Lehnert, *Inorg. Chem.* **2010**, *49*, 6293 – 6316.
[5] a) L. Cheng, G. B. Richter-Addo, *The Porphyrin Handbook Kadish*, *Vol. 4* (Eds.: K. M. Kadish, K. M. Smith, R. Guilard), Academic Press, New York, **2000**, Chap. 33, pp. 219 – 291; b) C. M. Coyle, K. M. Vogel, T. S. Rush, P. M. Kozlowski, R. Williams, T. G. Spiro, Y. Dou, M. Ikeda-Saito, J. S. Olson, M. Z. Zgierski, *Biochemistry* **2003**, *42*, 4896 – 4903; c) N. Lehnert, T. C. Berto, M. G. I. Galinato, L. E. Goodrich, in *The Handbook of Porphyrin Science,* Vol. 14, Chapter 63 (Eds.: K. M. Kadish, K. M. Smith, R. Guilard), World Scientific, Singapore, **2011**, pp. 1 – 247; d) N. J. Silvernail, A. Barabanschikov, J. T. Sage, B. C. Noll, W. R. Scheidt, *J. Am. Chem. Soc.* **2009**, *131*, 2131 – 2140; e) G. R. Wyllie, W. R. Scheidt, *Chem. Rev.* **2002**, *102*, 1067 – 1090; f) V. Praneeth, F. Neese, N. Lehnert, *Inorg. Chem.* **2005**, *44*, 2570 – 2572; g) M. Radoul, M. Sundararajan, A. Potapov, C. Riplinger, F. Neese, D. Goldfarb, *Phys. Chem. Chem. Phys.* **2010**, *12*, 7276 – 7289.
[6] a) J. P. Collman, Y. Yang, A. Dey, R. A. Decréau, S. Ghosh, T. Ohta, E. I. Solomon, *Proc. Natl. Acad. Sci. USA* **2008**, *105*, 15660 – 15665; b) T. C. Berto, M. B. Hoffman, Y. Murata, K. B. Landenberger, E. E. Alp, J. Zhao, N. Lehnert, *J. Am. Chem. Soc.* **2011**, *133*, 16714 – 16717; c) I. M. Wasser, H. Huang, P. Möenne-Loccoz, K. D. Karlin, *J. Am. Chem. Soc.* **2005**, *127*, 3310 – 3320; d) J. P. Collman, A. Dey, Y. Yang, R. A. Decréau, T. Ohta, E. I. Solomon, *J. Am. Chem. Soc.* **2008**, *130*, 16498 – 16499..
[7] a) N. Yeung, Y.-W. Lin, Y.-G. Gao, X. Zhao, B. S. Russell, L. Lei, K. D. Miner, H. Robinson, Y. Lu, *Nature* **2009**, *462*, 1079 – 1082; b) Y. Lu, N. Yeung, N. Sieracki, N. M. Marshall, *Nature* **2009**, *460*, 855 – 862; c) Y.-W. Lin, N. Yeung, Y.-G. Gao, K. D. Miner, S. Tian, H. Robinson, Y. Lu, *Proc. Natl. Acad. Sci. USA* **2010**, *107*, 8581 – 8586; d) Y.-W. Lin, N. Yeung, Y.-G. Gao, K. D. Miner, L. Lei, H. Robinson, Y. Lu, *J. Am. Chem. Soc.* **2010**, *132*, 9970 – 9972; e) Y. Lu, S. Chakraborty, K. D. Miner, T. D. Wilson, A. Mukherjee, Y. Yu, J. Liu, N. M. Marshall, *Comprehensive Inorganic Chemistry II* (Eds.: J. Reedijk, K. Poeppelmeier), Elsevier, Amsterdam, **2013**, pp. 565 – 593; f) T. Hayashi, K. D. Miner, N. Yeung, Y.-W. Lin, Y. Lu, P. Möenne-Loccoz, *Biochemistry* **2011**, *50*, 5939 – 5947.
[8] T. Hino, Y. Matsumoto, S. Nagano, H. Sugimoto, Y. Fukumori, T. Murata, S. Iwata, Y. Shiro, *Science* **2010**, *330*, 1666 – 1670.
[9] W. L. DeLano, The PyMOL Molecular Graphics System, DeLano Scientific, Palo Alto, California, USA **2005**, http://www.pymol.org.
[10] a) F. W. J. Teale, *Biochim. Biophys. Acta* **1959**, *35*, 543; b) T. Koshiyama, M. Shirai, T. Hikage, H. Tabe, K. Tanaka, S. Kitagawa, T. Ueno, *Angew. Chem.* **2011**, *123*, 4951 – 4954; *Angew. Chem. Int. Ed.* **2011**, *50*, 4849 – 4852; c) Z.-X. Liang, J. M. Nocek, K. Huang, R. T. Hayes, I. V. Kurnikov, D. N. Beratan, B. M. Hoffman, *J. Am. Chem. Soc.* **2002**, *124*, 6849 – 6859; d) N. Wang, X. Zhao, Y. Lu, *J. Am. Chem. Soc.* **2005**, *127*, 16541 – 16547.
[11] a) J. A. Sigman, B. C. Kwok, A. Gengenbach, Y. Lu, *J. Am. Chem. Soc.* **1999**, *121*, 8949 – 8950; b) J. A. Sigman, B. C. Kwok, Y. Lu, *J. Am. Chem. Soc.* **2000**, *122*, 8192 – 8196.
[12] P. D. Adams, P. V. Afonine, G. Bunkoczi, V. B. Chen, I. W. Davis, N. Echols, J. J. Headd, L.-W. Hung, G. J. Kapral, R. W. Grosse-Kunstleve, A. J. McCoy, N. W. Moriarty, R. Oeffner, R. J. Read, D. C. Richardson, J. S. Richardson, T. C. Terwilliger, P. H. Zwart, *Acta Crystallogr. Sect. D* **2010**, *66*, 213 – 221.
[13] J. Enemark, R. Feltham, *Coord. Chem. Rev.* **1974**, *13*, 339 – 406.
[14] P. Schmidt, R. Kappl, J. Hüttermann, *Appl. Magn. Reson.* **2001**, *21*, 423 – 440.
[15] H. Kumita, K. Matsuura, T. Hino, S. Takahashi, H. Hori, Y. Fukumori, I. Morishima, Y. Shiro, *J. Biol. Chem.* **2004**, *279*, 55247 – 55254.
[16] a) D. M. Arciero, J. D. Lipscornb, B. H. Huynh, T. A. Kent, E. Münck, *J. Biol. Chem.* **1983**, *258*, 14981 – 14991; b) B. D′Autréaux, N. P. Tucker, R. Dixon, S. Spiro, *Nature* **2005**, *437*, 769 – 772; c) B. S. Pierce, J. D. Gardner, L. J. Bailey, T. C. Brunold, B. G. Fox, *Biochemistry* **2007**, *46*, 8569 – 8578; d) A. M. Orville, V. J. Chen, A. Kriauciunas, M. R. Harpel, B. G. Fox, E. Münck, J. D. Lipscomb, *Biochemistry* **1992**, *31*, 4602 – 4612; e) J. H. Rodriguez, Y.-M. Xia, P. G. Debrunner, *J. Am. Chem. Soc.* **1999**, *121*, 7846 – 7863; f) Y. Zhang, M. A. Pavlosky, C. A. Brown, T. E. Westre, B. Hedman, K. O. Hodgson, E. I. Solomon, *J. Am. Chem. Soc.* **1992**, *114*, 9191 – 9192; g) J. M. Nocek, D. M. Kurtz, Jr., J. T. Sage, Y. M. Xia, P. Debrunner, A. K. Shiemke, J. Sanders-Loehr, T. M. Loehr, *Biochemistry* **1988**, *27*, 1014 – 1024.
[17] a) F. Wells, S. McCann, H. Wickman, S. Kessel, D. Hendrickson, R. Feltham, *Inorg. Chem.* **1982**, *21*, 2306 – 2311; b) C. A. Brown, M. A. Pavlosky, T. E. Westre, Y. Zhang, B. Hedman, K. O. Hodgson, E. I. Solomon, *J. Am. Chem. Soc.* **1995**, *117*, 715 – 732; c) M. Li, D. Bonnet, E. Bill, F. Neese, T. Weyhermüller, N. Blum, D. Sellmann, K. Wieghardt, *Inorg. Chem.* **2002**, *41*, 3444 – 3456; d) C. Hauser, T. Glaser, E. Bill, T. Weyhermüller, K. Wieghardt, *J. Am. Chem. Soc.* **2000**, *122*, 4352 – 4365; e) T. C. Berto, A. L. Speelman, S. Zheng, N. Lehnert, *Coord. Chem. Rev.* **2013**, *257*, 244 – 259.
[18] a) P. G. Debrunner in *Spectroscopic Approaches to Biomolecular Conformation* (Ed.: D. W. Urry), American Medical Association, Chicago, **1970**, pp. 209 – 262; b) N. N. Greenwood, T. C. Gibb, *Mossbauer Spectroscopy*, Chapman and Hall, London, **1971**.
[19] a) E. Bill, F.-H. Bernhardt, A. X. Trautwein, H. Winkler, *Eur. J. Biochem.* **1985**, *147*, 177 – 182; b) C. J. Haskin, N. Ravi, J. B. Lynch, E. Münck, L. Que, Jr., *Biochemistry* **1995**, *34*, 11090 – 11098; c) Y. Zhang, E. Oldfield, *J. Am. Chem. Soc.* **2004**, *126*, 9494 – 9495.
[20] Y. Zhang, E. Oldfield, *J. Phys. Chem. A* **2003**, *107*, 4147 – 4150.
[21] H. Matsumura, T. Hayashi, S. Chakraborty, Y. Lu, P. Möenne-Loccoz, *J. Am. Chem. Soc.* **2014**, DOI: 10.1021/ja410542z.

